Mössbauer Spectroscopy of Spin-Coupled Iron−Chromium Complexes: μ-Hydroxo−Bis(μ-acetato)-Bridged Iron(2+)−Chromium(3+) and μ-Oxo−Bis(μ-acetato)-Bridged Iron(3+)−Chromium(3+)

J. H. Rodriguez,*[1a] Y.-M. Xia,[1a] P. G. Debrunner,[1a] P. Chaudhuri,[1b] and K. Wieghardt[1b]

Contribution from the Department of Physics, University of Illinois at Urbana−Champaign, Urbana, Illinois 61801, and the Lehrstuhl für Anorganische Chemie I, Ruhr-Universität, D-4630 Bochum, Germany

Received July 26, 1995[⊗]

Abstract: We have analyzed Mössbauer spectra of a model complex of known structure with an $Fe^{2+}(S_1=2)-\mu OH-Cr^{3+}(S_2=3/2)$ center (**A**) and of its $Fe^{3+}(S_1=5/2)-\mu O-Cr^{3+}(S_2=3/2)$ analog (**B**). These μ-hydroxo and μ-oxo bridged binuclear metal centers display unusual magnetic properties as found in several diiron−oxo proteins. Our results confirm antiferromagnetic spin coupling between Fe and Cr ions which results in $S^{eff}=1/2$ and $S^{eff}=1$ ground states for **A** and **B**, respectively. The isotropic exchange $H_{ex}=J\mathbf{S}_1\cdot\mathbf{S}_2$ is weaker for the μ-hydroxo ($J\approx 21$ cm^{-1}) than for the μ-oxo ($J\approx 275$ cm^{-1}) complex. Spectra recorded at 4.2 K, in fields of 0.22−4.7 T, have been analyzed with the effective spin Hamiltonian for the ground state $H^{eff}=\beta\mathbf{S}^{eff}\cdot\tilde{g}^{eff}\cdot\mathbf{H}+\mathbf{S}^{eff}\cdot\tilde{A}_1^{eff}\cdot\mathbf{I}_1+\mathbf{I}_1\cdot\tilde{P}_1\cdot\mathbf{I}_1-\beta_n g_n\mathbf{H}\cdot\mathbf{I}_1$. For complex **B**, the zero-field splitting $\mathbf{S}^{eff}\cdot\tilde{D}^{eff}\cdot\mathbf{S}^{eff}$ is also included in H^{eff}. In applied fields, the 4.2 K spectra of Fe^{2+} in **A** showed hyperfine splittings which allowed the determination of the following $S^{eff}=1/2$ Hamiltonian parameters: $1/3$ Tr $\tilde{g}^{eff}\approx 2.00$, $\tilde{A}_1^{eff}/g_n\beta_n=-(18.3,5.6,25.0)$ T, $\Delta E_Q=+2.87$ mm/s, $\eta=0.93$, and $\delta_{Fe}=1.21$ mm/s. The weak coupling of **A** allows the zero-field splitting to mix higher spin manifolds with the ground state doublet, and, to obtain intrinsic parameters, we also calculated the spectra of Fe^{2+} by diagonalizing the $(2S_1+1=5)\times(2S_2+1=4)$ matrix of the Hamiltonian $H=J\mathbf{S}_1\cdot\mathbf{S}_2+\sum_{i=1}^{2}\{\mathbf{S}_i\cdot\tilde{D}_i\cdot\mathbf{S}_i+\beta\mathbf{S}_i\cdot\tilde{g}_i\cdot\mathbf{H}\}+\mathbf{S}_1\cdot\tilde{a}_1\cdot\mathbf{I}_1+\mathbf{I}_1\cdot\tilde{P}_1\cdot\mathbf{I}_1-\beta_n g_n\mathbf{H}\cdot\mathbf{I}_1$. We determined the following parameters for Fe^{2+}: $D_1=+4.0$ cm^{-1}, $E_1=+0.4$ cm^{-1}, $1/3$ Tr $\tilde{g}_1\gtrsim 2.07$, $\tilde{a}_1/g_n\beta_n=-(10.2,3.5,15.6)$ T. For complex **B**, we found that Fe^{3+} has a large quadrupole splitting ($\Delta E_Q=-2.00$ mm/s, $\eta=0.22$) presumably as a result of anisotropic covalency due to the close proximity of the bridging O^{2-}. This large ΔE_Q is comparable to values found in diiron−oxo proteins. Spectra of **B** in applied fields also displayed hyperfine splittings, and the following $S^{eff}=1$ Hamiltonian parameters could be deduced: $D^{eff}=+3.9$ cm^{-1}, $E^{eff}=+1.7$ cm^{-1}, $1/3$ Tr $\tilde{g}^{eff}=2.01$, $\tilde{A}_1^{eff}/g_n\beta_n=-(33.8,30.9,35.8)$ T, $\delta_{Fe}=0.52$ mm/s.

I. Introduction

The synthesis, magnetic properties, and structures of μ-hydroxo−bis(μ-acetato)- and μ-oxo−bis(μ-acetato)-bridged iron−chromium model compounds have been reported by Chaudhuri *et al.*[2] and Hotzelmann *et al.*,[3] respectively. The metal centers of these complexes mimic the structure of a number of diiron−oxo proteins, such as hemerythrin,[4] methane monooxygenase,[5] and ribonucleotide reductase,[6] which have been structurally characterized. Most importantly, in analogy to diiron−oxo proteins, the bridging units of these complexes constitute superexchange pathways which allow antiferromagnetic coupling between the spins of iron and chromium.

The first complex (**A**), with formula $[LCr(\mu\text{-}OH)(\mu\text{-}CH_3COO)_2FeL](ClO_4)_2$ (L = $C_9H_{21}N_3$), has $Fe^{2+}(S_1=2)$ and $Cr^{3+}(S_2=3/2)$ ions which interact through one hydroxo and two μ-acetato bridges.[2] The two metal ions have distorted octahedral geometry. The bridging OH^- is separated from Fe^{2+} and Cr^{3+} by 2.037 and 1.924 Å, respectively.[2] The $Fe^{2+}-Cr^{3+}$ distance is 3.413 Å.

The bridging pathways and the close proximity of the metal ions in **A** allow weak antiferromagnetic spin coupling which produces a $S^{eff}=2-3/2=1/2$ ground state. Such behavior has been verified by variable temperature magnetic susceptibility measurements which yield a coupling constant[2] of $J\approx 21$ cm^{-1} for the isotropic exchange interaction.

$$H_{ex}=J\mathbf{S}_1\cdot\mathbf{S}_2 \tag{1}$$

A second complex (**B**), with formula $[L'Cr(\mu\text{-}O)(\mu\text{-}CH_3COO)_2FeL](PF_6)_2$ (L′ = $C_9H_{21}N_3$, L = $C_6H_{15}N_3$), has $Fe^{3+}(S_1=5/2)$ and $Cr^{3+}(S_2=3/2)$ ions strongly antiferromagnetically coupled through one oxo and two μ-acetato bridges.[3] Here, the antiferromagnetic exchange is on the order of $J\approx 275$ cm^{-1} according to magnetic susceptibility[3] and produces a $S^{eff}=5/2-3/2=1$ ground state. In complex **B** the bridging O^{2-} is separated from Fe^{3+} and Cr^{3+} by 1.792 and 1.798 Å, respectively,[3] and the $Fe^{3+}-Cr^{3+}$ distance is 3.126 Å.

The mechanism of antiferromagnetic spin coupling in metalloproteins was first applied by Gibson *et al.*[7] in order to explain the EPR spectrum of spinach ferredoxin, a 2Fe−2S protein. The

[⊗] Abstract published in *Advance ACS Abstracts,* August 1, 1996.

(1) (a) University of Illinois at Urbana−Champaign. (b) Ruhr-Universität. Presently at Max-Planck-Institut für Strahlenchemie, Stiftstrasse 34−36, D-45470 Mülheim an der Ruhr, Germany.

(2) Chaudhuri, P.; Winter, M.; Küppers, H. J.; Wieghardt, K.; Nuber, B.; Weiss, J. *Inorg. Chem.* **1987**, *26*, 3302.

(3) Hotzelmann, R.; Wieghardt, K.; Flörke, U.; Haupt, H.-J.; Weatherburn, D.; Bonvoisin, J.; Blondin, G.; Girerd, J. *J. Am. Chem. Soc.* **1992**, *114*, 1683.

(4) Stenkamp, R. E.; Sieker, L. C.; Jensen, L. H. *J. Am. Chem. Soc.* **1984**, *106*, 618.

(5) Rosenzweig, A. C.; Frederick, C. A.; Lippard, S. J.; Nordlund, P. *Nature* **1993**, *366*, 537.

(6) Nordlund, P.; Sjöberg, B. M.; Eklund, H. *Nature* **1990**, *345*, 593.

S0002-7863(95)02513-3 CCC: $12.00

same mechanism greatly influences the spectroscopic and magnetic properties, determined by several techniques such as EPR and magnetic susceptibility, of diiron−oxo proteins and related model complexes.[8−11]

Mössbauer spectroscopy is valuable to the study of spin-coupled metal centers. In addition to the isomer shifts and electric quadrupole interactions $\mathbf{I}\cdot\tilde{P}\cdot\mathbf{I}$, which together characterize the oxidation and spin state of the iron sites, spectra recorded in external fields and at low temperatures (e.g., $T \lesssim 4.2$ K) are sensitive to the magnetic hyperfine interactions $\mathbf{S}^{\text{eff}}\cdot\tilde{A}^{\text{eff}}\cdot\mathbf{I}$ and, for $S^{\text{eff}} \geq 1$, to the zero-field splittings (ZFS) $\mathbf{S}^{\text{eff}}\cdot\tilde{D}^{\text{eff}}\cdot\mathbf{S}^{\text{eff}}$ arising from the spin ground states of paramagnetic irons in exchange-coupled centers.[8,11]

In this work we report the analysis of spectra from complexes **A** and **B**, recorded in external fields of 0.22 to ≈4.7 T, in terms of effective spin Hamiltonians for their ground states. Spectra of the Fe^{2+} site of **A**, in the 4.2−7 K range, have been interpreted as arising from a $S^{\text{eff}} = {}^1/_2$ Kramers doublet. Spectra of the Fe^{3+} site of complex **B** at 4.2 K have been interpreted as resulting from a $S^{\text{eff}} = 1$ ground state. In addition, we present the analysis of the 4.2 K spectra from complex **A** in terms of an intrinsic spin Hamiltonian that includes the isotropic exchange and zero-field splittings.

II. The Spin Hamiltonian

The main interactions that affect the electronic and nuclear environments of a spin coupled Fe−Cr pair are given by the spin Hamiltonian

$$H = H_{\text{el}} + H_{\text{nu}} \tag{2}$$

$$H_{\text{el}} = J\mathbf{S}_1\cdot\mathbf{S}_2 + \sum_{i=1}^{2}\{\mathbf{S}_i\cdot\tilde{D}_i\cdot\mathbf{S}_i + \beta\mathbf{S}_i\cdot\tilde{g}_i\cdot\mathbf{H}\} \tag{3}$$

$$H_{\text{nu}} = \mathbf{S}_1\cdot\tilde{a}_1\cdot\mathbf{I}_1 + \mathbf{I}_1\cdot\tilde{P}_1\cdot\mathbf{I}_1 - \beta_n g_n\mathbf{H}\cdot\mathbf{I}_1 \tag{4}$$

where the electronic Hamiltonian H_{el} includes the isotropic exchange, ZFS, and electronic Zeeman interactions, in the intrinsic spin representation, of Fe (site 1) and Cr (site 2), respectively. The nuclear Hamiltonian H_{nu} includes the magnetic hyperfine, electric quadrupole, and nuclear Zeeman interactions and has been written for the Mössbauer isotope ^{57}Fe only. We assume the inequality $\langle H_{\text{el}}\rangle \gg \langle H_{\text{nu}}\rangle$.

If the antiferromagnetic exchange term in eq 3 is dominant, the low-temperature (e.g., $T \lesssim 4.2$ K) properties of the pair can be ascribed to an isolated ground spin manifold ($S^{\text{eff}} = S_1 - S_2$) which is separated from the higher manifolds according to

$$E(S) - E(S-1) = JS \tag{5}$$

Equation 5 gives the energy difference between two states of the exchange interaction (eq 1) corresponding to the eigenvalues S and $S-1$ of the total spin operator $\mathbf{S} = \mathbf{S}_1 + \mathbf{S}_2$. For $kT \ll JS^{\text{eff}}$, only the ground state is significantly populated. In this case, it is appropriate to express the Hamiltonian (eq 2) in terms of the effective spin operator $\mathbf{S}^{\text{eff}} = \mathbf{S}_1 - \mathbf{S}_2$, and Mössbauer spectra of the coupled system can be analyzed with the following effective spin Hamiltonian for the ground state:

$$H^{\text{eff}} = \mathbf{S}^{\text{eff}}\cdot\tilde{D}^{\text{eff}}\cdot\mathbf{S}^{\text{eff}} + \beta\mathbf{S}^{\text{eff}}\cdot\tilde{g}^{\text{eff}}\cdot\mathbf{H} + \mathbf{S}^{\text{eff}}\cdot\tilde{A}_1^{\text{eff}}\cdot\mathbf{I}_1 + \mathbf{I}_1\cdot\tilde{P}_1\cdot\mathbf{I}_1 - \beta_n g_n\mathbf{H}\cdot\mathbf{I}_1 \tag{6}$$

where $\tilde{D}^{\text{eff}}$, $\tilde{g}^{\text{eff}}$, and $\tilde{A}_1^{\text{eff}}$ are the tensors, in the effective spin representation, corresponding to the ZFS, electronic Zeeman, and magnetic hyperfine interactions, respectively. In this way, the interpretation of the low-temperature Mössbauer spectra of an Fe−Cr pair rests on the determination of the parameters of eq 6. For the analysis of complex **A**, the term $\mathbf{S}^{\text{eff}}\cdot\tilde{D}^{\text{eff}}\cdot\mathbf{S}^{\text{eff}}$ in eq 6 is omitted since it does not remove the degeneracy of the $S^{\text{eff}} = {}^1/_2$ Kramers doublet.

From an application of the Wigner−Eckart theorem, the matrix elements of a tensor operator of operator variable $\mathbf{S}_i$ are proportional to those of the tensor operator of the same rank with operator variable $\mathbf{S}$. It follows that the matrix elements of the interactions of eq 2 are equal to those of eq 6 when intrinsic and effective tensors are related by proper proportionality constants. For strong exchange coupling ($|J/D_i| \gg 1$), the following relations hold:[12−14]

$$\tilde{g}^{\text{eff}} = \sum_{i=1}^{2} C_i\tilde{g}_i$$

$$\tilde{A}_1^{\text{eff}} = C_1\tilde{a}_1 \tag{7}$$

where the proportionality constants C_i are, in general, specific for each spin manifold and equal to the ratio of the reduced matrix elements in effective and intrinsic representations.

For $S^{\text{eff}} = {}^1/_2$, $S_1 = 2$, and $S_2 = {}^3/_2$, expressions 7 can be explicitly written as

$$\tilde{g}^{\text{eff}} = +2\tilde{g}_1 - \tilde{g}_2 \tag{8}$$

$$\tilde{A}_1^{\text{eff}} = +2\tilde{a}_1 \tag{9}$$

Similarly, for $S^{\text{eff}} = 1$, $S_1 = {}^5/_2$, and $S_2 = {}^3/_2$, expressions 7 are

$$\tilde{g}^{\text{eff}} = +{}^7/_4\tilde{g}_1 - {}^3/_4\tilde{g}_2 \tag{10}$$

$$\tilde{A}_1^{\text{eff}} = +{}^7/_4\tilde{a}_1 \tag{11}$$

The intrinsic tensors $\tilde{D}_i$ of eq 3 are chosen to be traceless, and the zero-field splittings are given in terms of the axial (D_i) and rhombic (E_i) parameters

$$H_{\text{ZFS}} = \sum_{i=1}^{2}\{D_i[S_{zi}^2 - {}^1/_3S_i(S_i+1)] + E_i(S_{xi}^2 - S_{yi}^2)\} \tag{12}$$

where the following relations hold:

$$D_i = {}^3/_2D_{zzi}$$

$$E_i = {}^1/_2(D_{xxi} - D_{yyi}) \tag{13}$$

The ZFS defines the system of axes for each metal ion. We follow Blumberg[15] and choose a proper coordinate system by letting z be the axis that makes D_i largest in magnitude and

(7) Gibson, J. F.; Hall, D. O.; Thornley, J. H. M.; Whatley, F. R. *Proc. Natl. Acad. Sci. U.S.A.* **1966**, *56*, 987.
(8) Debrunner, P. G. *Hyperfine Interact.* **1990**, *53*, 21.
(9) Que, L., Jr.; True, A. E. *Prog. Inorg. Chem.* **1990**, *38*, 97.
(10) Vincent, J. B.; Olivier-Lilley, G. L.; Averill, B. A. *Chem. Rev.* **1990**, *90*, 1447.
(11) Debrunner, P. G. In *Biological Magnetic Resonance: EMR of Paramagnetic Molecules*; Berliner, L. J., Reuben, J., Eds.; Plenum Press: New York, 1993; Vol. 13.
(12) Scaringe, P. R.; Derek, J. H.; Hatfield, W. E. *Mol. Phys.* **1978**, *35*, 701.
(13) Bencini, A.; Gatteschi, D. *EPR of Exchange Coupled Systems*; Springer-Verlag: Berlin, 1990.
(14) Kahn, O. *Molecular Magnetism*; VCH: New York, 1993.
(15) Blumberg, W. E. In *Magnetic Resonance in Biological Systems*; Ehrenberg, A., Malmström, B. G., Vängard, T., Eds.; Pergamon: Oxford; 1967.

constraining D_i and E_i to have equal signs. This choice is consistent with the conditions $|D_{zz}| \geq |D_{yy}| \geq |D_{xx}|$, and $0 \leq E/D \leq {}^1/_3$.

Similarly, we express the interaction $\mathbf{S}^{\text{eff}}\cdot\tilde{D}^{\text{eff}}\cdot\mathbf{S}^{\text{eff}}$ of eq 6 representing the ZFS for a $S^{\text{eff}} = 1$ manifold as follows

$$H^{\text{eff}}_{\text{ZFS}} = D^{\text{eff}}[S_z^2 - {}^2/_3] + E^{\text{eff}}(S_x^2 - S_y^2) \qquad (14)$$

where S_x, S_y, and S_z are the components of $\mathbf{S}^{\text{eff}}$. D^{eff} and E^{eff} are the axial and rhombic contributions, respectively, related to the principal values of $\tilde{D}^{\text{eff}}$ by expressions 13 if we substitute effective for intrinsic parameters.

For $E^{\text{eff}} = 0$ and $D^{\text{eff}} > 0$, the $S^{\text{eff}} = 1$ triplet is split into a higher doublet and a lower singlet. Addition of the rhombic term removes the degeneracy of the higher doublet separating its two sublevels by $2E^{\text{eff}}$.

Electric Quadrupole Interaction. The nuclear excited state quadrupole moment interacts with two main sources of electric field gradient (EFG). First, there is a contribution from the nonspherical valence electronic charge of the d electrons of the iron ion. Second, some EFG arises from noncubic charge distributions of the lattice about the ion. In addition, for some complexes, covalency introduces a third contribution to the EFG by inducing an anisotropic electron population of the valence molecular orbitals.[16] For high-spin Fe^{3+} the EFG arises from lattice and/or covalent contributions whereas the valence component is nominally zero. By contrast, for high-spin Fe^{2+} the lattice and covalent effects, if present, constitute a relatively small perturbation to the dominant valence contribution to the EFG.

The electric quadrupole interaction $\mathbf{I}_1\cdot\tilde{P}_1\cdot\mathbf{I}_1$ for each iron site is more explicitly given by

$$H_{E_Q} = \frac{eQV_{zz}}{12}[3I_z^2 - I(I+1) + \eta(I_x^2 - I_y^2)] \qquad (15)$$

where e is the charge of the proton, Q is the nuclear quadrupole moment, and $-V_{zz}$ is the principal component of the traceless EFG tensor $-\tilde{V}$ in its principal axes.

The asymmetry parameter η that represents a departure from axial symmetry is

$$\eta = \frac{V_{xx} - V_{yy}}{V_{zz}} \qquad (16)$$

where $0 \leq \eta \leq 1$ is obtained with the convention $|V_{zz}| > |V_{yy}| \geq |V_{xx}|$.

^{57}Fe has nuclear spins $I_g = {}^1/_2$ and $I_e = {}^3/_2$ for its ground and excited states, respectively. When the electric field gradient at the nuclear site has axial symmetry, diagonalization of the electric quadrupole interaction yields two nonvanishing diagonal matrix elements for the $|\pm{}^3/_2\rangle$ and $|\pm{}^1/_2\rangle$ sublevels of the $I_e = {}^3/_2$ multiplet. The energy difference between these two sublevels, which is directly measured by Mössbauer spectroscopy, is the quadrupole splitting ΔE_Q. In general, for asymmetric field gradients at the nucleus we have

$$\Delta E_Q = {}^1/_2 eQV_{zz}(1 + \eta^2/3)^{1/2} \qquad (17)$$

In the principal axes of the EFG tensor, all nondiagonal terms V_{ij} ($i \neq j$) vanish. For Fe^{2+}, the diagonal (principal) terms of the dominant valence contribution to the EFG tensor for a single d electron are given by

$$V_{ii} = {}^2/_7 e(1 - R)\langle r^{-3}\rangle\langle d_1|L_{ii}^2 - 2|d_1\rangle \qquad (18)$$

where $(1 - R)$ is the Sternheimer factor,[17] $\langle r^{-3}\rangle$ is the mean value of r^{-3} for 3d electrons,[18,19] and L_{ii} are the components of the orbital angular momentum operator. In eq 18, the expectation values $\langle d_1|L_{ii}^2 - 2|d_1\rangle$ are evaluated for the ferrous ground state orbital d_1 which accommodates two paired electrons.

III. Materials and Methods

We recorded Mössbauer spectra for powder and solution samples containing complexes **A** and **B** for the temperature range 1.8 K $\lesssim T \lesssim$ 200 K in zero and applied external magnetic fields. The analysis performed for powder samples revealed that the iron sites of **A** and **B** did not achieve the limit of slow relaxation at 4.2 K in low fields (e.g., 0.22 T). For solution samples, the ferric site of **B** displayed slow relaxation at 4.2 K in a 0.22 T field, whereas the ferrous site of **A** required higher fields to reach this limit. The relaxation rates are further discussed in section V. In this study we focused on solution samples of **A** and **B** since these allowed us to achieve slow relaxation with the available fields and temperatures. The preparation of X-ray quality crystals of complexes **A** and **B** was reported elsewhere.[2,3] The samples used in this work were acetonitrile solutions of polycrystalline unenriched **A** and **B** with iron concentrations on the order of 100 mM.

Mössbauer spectra recorded in applied fields of 0.032 to ≈4.7 T were obtained from frozen solution samples with a spectrometer that operates in constant acceleration mode. The resulting data were analyzed with a program that calculates spectra of ^{57}Fe by diagonalizing the effective spin Hamiltonian of eq 6 in a way similar to that reported by Münck *et al*.[20] The spectra of **A** were also simulated in the intrinsic formalism with a code that diagonalizes eq 2.[21] Zero field spectra were analyzed with a least squares program that calculates a sum of Lorentzians.[22] As discussed below (section IV), the presence of two impurity iron species in the sample containing complex **A** required the simultaneous simulation of three different spectra. Therefore, it was necessary to determine a large number of parameters in order to reproduce the experimental data. To find an optimal set of parameters we searched in the parameter space of eq 6 with a genetic algorithm as described elsewhere.[21] The genetic algorithm has allowed us to simulate data with great detail.

EPR spectra of the acetonitrile solution of polycrystalline **A** ($Fe^{2+}-\mu OH-Cr^{3+}$) were recorded on a Bruker ER 200 X-band spectrometer at 4.2 K. The same sample was studied by Mössbauer spectroscopy before it was transferred to the EPR tube in a glovebox.

IV. Results

A careful analysis of Mössbauer spectra from frozen solution samples of complex **A** ($Fe^{2+}-\mu OH-Cr^{3+}$) revealed that its high-spin Fe^{2+} site accounts for only 62% of the total spectral area. Lorentzian fits of 4.2 K spectra in zero field (Figure 1) showed two additional impurity iron species which displayed two partially resolved ferric quadrupole doublets as indicated in Table 1. One of the ferric species (impurity A), with parameters $\delta_{\text{Fe}} = 0.50$ mm/s, $\Delta E_Q = -1.53$ mm/s,[23] showed diamagnetic behavior in 2.2 and 4.2 T fields and contributed 16% of the spectral area. Spectra from the diamagnetic impurity arise from antiferromagnetic coupling between the ions of a diferric center. Such a coupling induces a system $S^{\text{eff}} = 0$

(16) Gütlich, P. In *Mössbauer Spectroscopy*; Gonser, U., Ed.; Springer-Verlag: Berlin, Heidelberg, New York, 1975.

(17) Sternheimer, R. M. *Phys. Rev.* **1963**, *130*, 1423.

(18) Zimmermann, R. Ph.D. Thesis, Universitat Erlangen-Nürnberg, Dresden, 1973.

(19) Zimmermann, R. *Chem. Phys.* **1974**, *4*, 133.

(20) Münck, E.; Groves, J. L.; Tumolillo, T.; Debrunner, P. G. *Comput. Phys. Commun.* **1973**, *5*, 225.

(21) Rodriguez, J. H.; Ok, H. N.; Xia, Y. M.; Debrunner, P. G.; Hinrichs, B. E.; Meyer, T.; Packard, N. *J. Phys. Chem.* **1996**, *100*, 6849.

(22) Chrisman, B. L.; Tumolillo, T. A. *Comput. Phys. Commun.* **1971**, *2*, 322.

(23) We follow the convention that the sign of ΔE_Q is given by the sign of V_{zz} which is obtained from simulations in applied field.

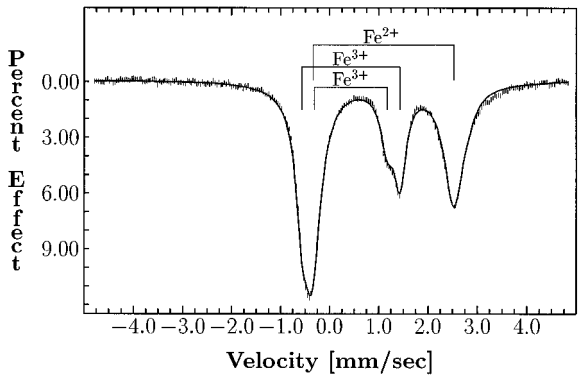

Figure 1. Spectrum of sample containing complex **A** ($Fe^{2+}-\mu OH-Cr^{3+}$) recorded in zero field at 4.2 K. The solid line is the Lorentzian fit for the Fe^{2+} doublet and impurities. Mössbauer parameters for the Fe^{2+} site of **A** are given in Table 2. Parameters for impurities are given in Table 1. The inner and outer brackets for Fe^{3+} represent the doublets corresponding to the $S^{eff} = 0$ and $S^{eff} = 1$ impurities, respectively.

Table 1. Parameters for Impurity Species Present in Sample Containing Complex **A** ($Fe^{2+}-\mu OH-Cr^{3+}$) Obtained from Simulations of Zero- and Applied-Field Spectra at 4.2 K

	impurity A Fe^{3+}	impurity B[a] Fe^{3+}
S^{eff}	0	1
δ_{Fe} (mm/s)[b]	0.50	0.52
ΔE_Q (mm/s)	−1.53	−2.00
Γ (mm/s)[c]	0.32	0.32
% area[d]	16	22

[a] The parameters for the Fe^{3+}(S^{eff}=1) species are similar to those presented for the ferric site of complex **B** in Table 2. [b] Isomer shifts with respect to iron metal at room temperature. [c] Γ is the full width at half maximum of the calculated intensities. [d] % area is the approximate percentage of the total spectral area for each iron species.

ground state which produces no magnetic hyperfine splitting in applied fields. The second ferric species (impurity B) contributed 22% of the area and presented magnetic structure in applied fields with parameters (Table 1) very similar to those found for the ferric site of complex **B**. The sample of complex **B** was found to be pure since only one iron species was observed in the zero-field spectrum as shown in Figure 3a.

The 4.2 K EPR spectra of **A** (not shown) displayed a single broad signal with a zero crossing at $g \approx 2.00$, and a peak-to-trough width of 32 mT. The 4.2 K Mössbauer spectra of the iron sites of complexes **A** and **B** were successfully simulated by finding sets of $S^{eff} = {}^1/_2$ and $S^{eff} = 1$ Hamiltonian parameters, respectively. These results are presented in Table 2, and the corresponding simulations are shown in Figures 2−4. In each case, isomer shifts, quadrupole splittings, and magnetic hyperfine tensors were obtained. For the ferric site of complex **B** the ZFS parameters D^{eff} and E^{eff} were found. The electric quadrupole interactions for the iron sites of **A** and **B** did not share principal axes with the other interactions in the Hamiltonian. The relative orientations of the $\tilde{P}$ tensors were found (Table 2) in terms of Euler angles following the convention of Brink and Satchler.[24] We also allowed the relative orientation of $\tilde{D}^{eff}$ to change with respect to that of g^{eff} and $\tilde{A}^{eff}$; however, the quality of the simulations did not improve. Instead, we found that the simulations are consistent with the tensors $\tilde{g}^{eff}$, $\tilde{A}^{eff}$, and $\tilde{D}^{eff}$ being coaxial for complexes **A** and **B**.

The 4.2 K Mössbauer spectra of **A** were also calculated in the intrinsic formalism of eq 2, and intrinsic parameters for the ZFS, magnetic hyperfine interaction, and $\tilde{g}_1$ of Fe^{2+} were found

Table 2. Effective Parameters for Fe^{2+} of Complex **A** ($Fe^{2+}-\mu OH-Cr^{3+}$) and Fe^{3+} of complex **B** ($Fe^{3+}-\mu O-Cr^{3+}$) Obtained from Simulations of Zero- and Applied-Field Mössbauer Spectra at 4.2 K with Eq 6

	complex **A** Fe^{2+}	complex **B** Fe^{3+}
S^{eff}	${}^1/_2$	1
δ_{Fe} (mm/s)[a]	1.21	0.52
ΔE_Q (mm/s)[23]	+2.87	−2.00
η	0.93	0.22
${}^1/_3$ Tr $\tilde{g}^{eff}$	2.00	2.01
$\tilde{A}^{eff}/g_n\beta_n$ (T)	−(18.3,5.6,25.0)	−(33.8,30.9,35.8)
$R(\tilde{A}^{eff} \rightarrow \tilde{P})$ (deg)[b]	(56,90,22)	(34,12,0)
Γ (mm/s)[c]	0.36	0.32
D^{eff} (cm^{-1})		+3.9[d]
E^{eff} (cm^{-1})		+1.7[d]

[a] Isomer shifts with respect to iron metal at room temperature. [b] Euler angles that rotate the principal axes of $\tilde{D}^{eff}$, $\tilde{g}^{eff}$, and $\tilde{A}^{eff}$ into those of $\tilde{P}$. [c] Γ is the full width at half maximum of the calculated intensities. [d] Since $E^{eff}/D^{eff} > 1/3$, the ZFS can be expressed with respect to a new proper axis system in order to obtain the condition $0 \le E/D \le 1/3$.

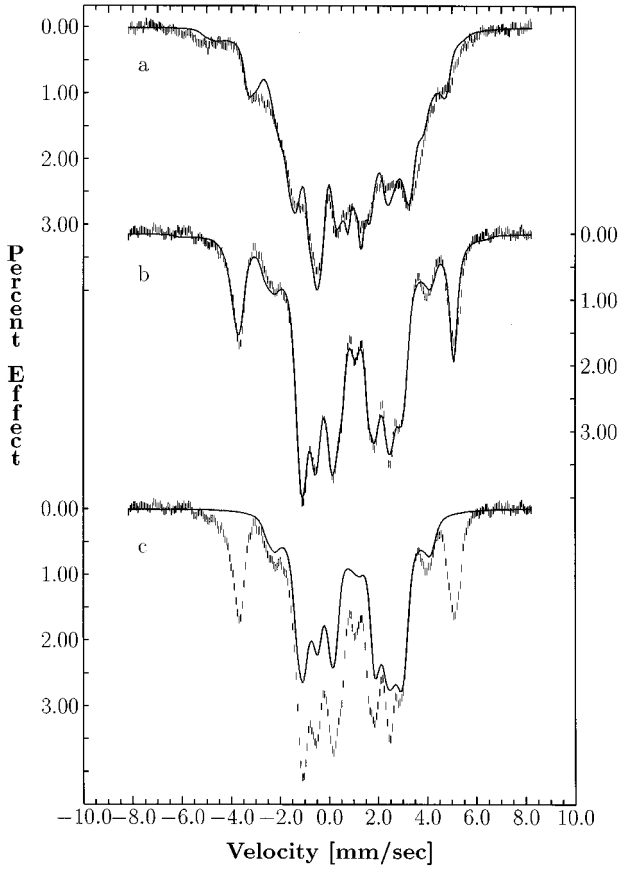

Figure 2. Spectra of sample containing complex **A** ($Fe^{2+}-\mu OH-Cr^{3+}$) obtained at 4.2 K in fields parallel to the γ beam of (a) 2.2 T and (b) 4.4 T. The solid lines are the combined simulations of all three iron species present in the sample. Parameters for the impurities are given in Table 1. Parameters for the Fe^{2+} site of **A** are given in Table 2. (c) Calculated spectra of the Fe^{2+} site of complex **A** for the 4.4 T spectrum. The solid line is a $S^{eff} = {}^1/_3$ simulation.

(Table 3). The intrinsic ZFS parameters for Cr^{3+} were only approximately determined since the simulations of Fe^{2+} Mössbauer spectra are not very sensitive, via eq 3, to small variations of D_2 and E_2. This observation is related to the small ZFS expected for Cr^{3+} [25] (section V) in comparison to that expected for Fe^{2+}.[21,26]

(24) Brink, D. M.; Satchler, G. R. *Angular Momentum*; Clarendon Press: Oxford, 1968.

(25) Buckmaster, H. A. *Magn. Reson. Rev.* **1986**, *11*, 99.

(26) Sage, J. T.; Xia, Y.-M.; Debrunner, P. G.; Keough, D. T.; de Jersey, J.; Zerner, B. *J. Am. Chem. Soc.* **1989**, *111*, 7239.

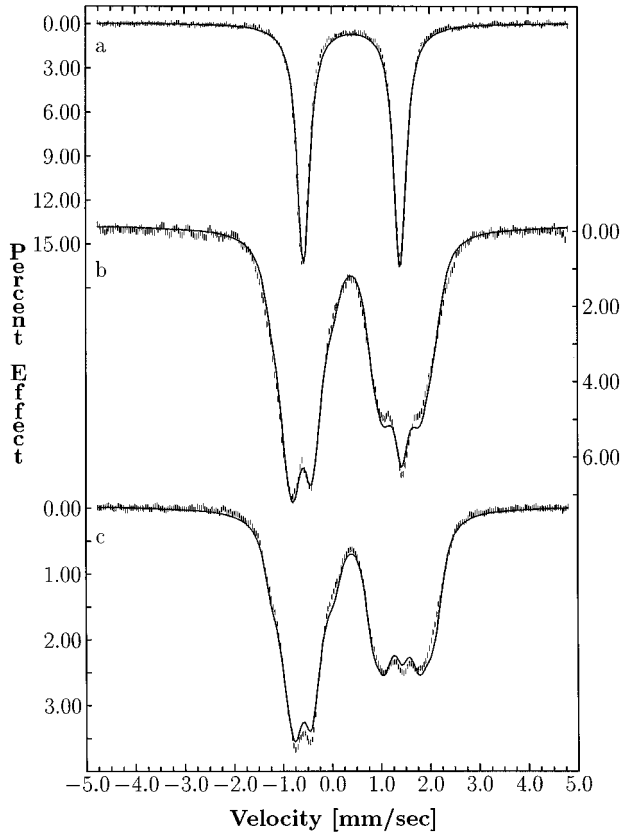

Figure 3. Spectra of Fe^{3+} from complex **B** ($Fe^{3+}-\mu O-Cr^{3+}$) recorded at 4.2 K in external fields relative to the incident γ beam of (a) zero field, (b) 0.22 T perpendicular, and (c) 0.22 T parallel. The solid lines are $S^{eff} = 1$ simulations with parameters given in Table 2.

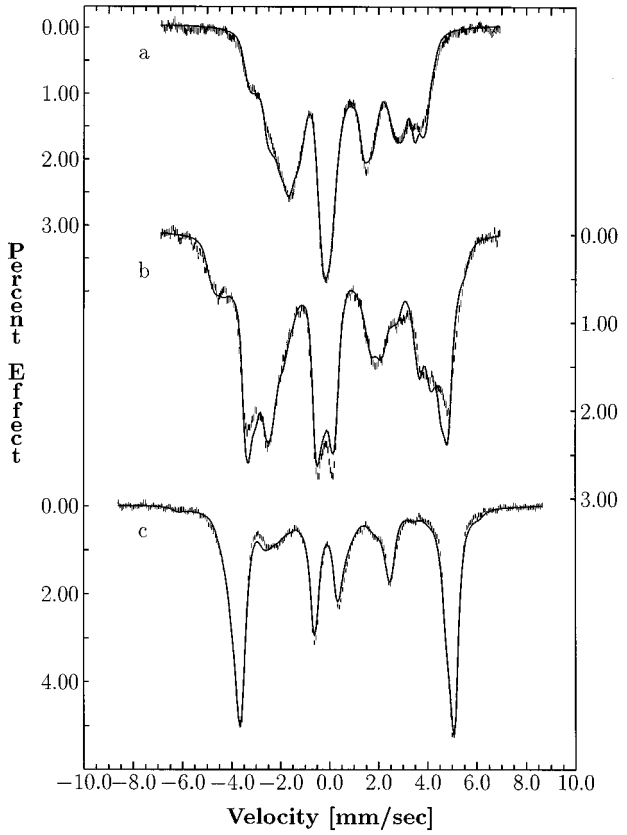

Figure 4. Spectra of Fe^{3+} from complex **B** ($Fe^{3+}-\mu O-Cr^{3+}$) recorded at 4.2 K in external fields relative to the incident γ beam of (a) 0.96 T parallel, (b) 1.9 T parallel, and (c) 4.7 T parallel. The solid lines are $S^{eff} = 1$ simulations with parameters given in Table 2.

V. Discussion

In what follows we briefly rationalize the spin Hamiltonian parameters obtained as well as some of the features of the spectra.

Complex A: $Fe^{2+}-\mu OH-Cr^{3+}$. The simulations shown in Figures 1 and 2 were performed assuming slow relaxation of electron spins, which corresponds to a stationary internal magnetic field acting on the nuclear moment. In this relaxation regime, the calculated spectral contributions arise from the two $M_S = \pm^1/_2$ substates of the ground Kramers doublet. Each spin substate gives rise to a well-defined spectrum with intensities proportional to their respective Boltzmann factors. The total calculated spectrum is the weighted sum of the two contributions. For a 4.4 T field, in the temperature range 4.2−7 K, the simulations were consistent with slow relaxation. At higher temperatures (e.g., >10 K), spectra showed triangular patterns which indicate intermediate relaxation. Finally, for temperatures greater than 40 K only fast relaxing spectra were observed. We notice that at 4.2 K, in 0.032 and 0.22 T fields, slow relaxation was not achieved. Instead, in low fields the broad features of experimental data contrasted greatly with the sharper features of the simulations, a behavior characteristic of intermediate spin relaxation.

As shown in Figure 1, the iron site of **A** displays at 4.2 K in zero field a quadrupole doublet with parameters $\delta_{Fe} = 1.21$ mm/s and $\Delta E_Q = +2.87$ mm/s[23] (Table 2). These parameters are consistent with the high spin state and the distorted octahedral environment[2] of the ferrous ion.[27−29] The triplet structure on the left side of the velocity scale (Figure 2c) is indicative of a negative sign for the largest component $-V_{zz}$ of the electric field gradient (i.e., V_{zz} is positive). For Fe^{2+} the main contribution to the EFG arises from the nonspherical valence electronic charge, in particular from the electron with spin antiparallel (↓) to the spins of the other five electrons in the high-spin configuration $d_1^{\uparrow\downarrow}d_2^{\uparrow}d_3^{\uparrow}d_4^{\uparrow}d_5^{\uparrow}$. According to eq 18, the positive sign of V_{zz} is intimately related to the symmetry of the ground state orbital d_1 and identifies it as the t_{2g} $|x^2 - y^2\rangle$ (with respect to an orthorhombic coordinate system rotated about the *z* axis of the octahedral potential). However, the large value of the asymmetry parameter ($\eta \approx 0.90 \leftrightarrow 0.93$) suggests that the orbital ground state is composed of an admixture of valence orbitals, presumably with a dominant orbital that yields a positive V_{zz}. In particular, an orthorhombic field can mix the e_g $|z^2\rangle$ and t_{2g} $|x^2 - y^2\rangle$ orbitals to yield the ground state[21,30] $\psi_1 = \alpha_0|x^2 - y^2\rangle + \beta_0|z^2\rangle$ ($\alpha_0^2 + \beta_0^2 = 1$ and $\alpha_0^2 \gg \beta_0^2$). Such an admixture of states can give rise to a sizable asymmetry parameter which can be calculated from eq 16 as[21] $\eta = 2\sqrt{3}\alpha_0\beta_0/(\alpha_0^2 - \beta_0^2)$. The expression for η shows that even small admixtures of the $|z^2\rangle$ orbital can produce large asymmetries of the ferrous EFG.

Effective Representation. The $S^{eff} = {}^1/_2$ simulations of 4.2 K spectra recorded in external fields of 2.2 and 4.4 T for the Fe^{2+} site of **A** and impurities are presented in Figure 2a,b. In spite of the complexity involved in simulating three different iron species simultaneously, we obtained close agreement between calculated and experimental spectra. Figure 2c shows the calculated contribution from the Fe^{2+} site of **A** to the 4.4 T

(27) Greenwood, N. N.; Gibb, T. C. *Mössbauer Spectroscopy*; Chapman and Hall: London, 1971.

(28) Debrunner, P. G. In *Spectroscopic Approaches to Biomolecular Conformation*; Urry, D. W., Ed.; A. M. A. Press: Chicago, 1970; Chapter 6, pp 209−262.

(29) Lang, G. *Q. Rev. Biophys.* **1970**, *3*, 1.

(30) Abragam, A.; Boutron, F. *C. R. Hebd. Seances Acad. Sci.* **1961**, *252*, 2404.

Table 3. Intrinsic Parameters of Fe^{2+} from Complex **A** ($Fe^{2+}-\mu OH-Cr^{3+}$) Obtained from Simulations of Mössbauer Spectra by Diagonalization of Eq 2[a,b]

S_1	J (cm^{-1})	D_1 (cm^{-1})	E_1 (cm^{-1})	$^1/_3$ Tr $\tilde{g}_1$	k[c]	λ (cm^{-1})	$\tilde{a}_1$ (T)	$R(\tilde{a}_1 \rightarrow \tilde{P})$ (deg)[d]	η
2	21[e]	+4.0	+0.4	$\gtrsim$2.07	0.8	−103	−(10.2,3.5,15.6)	(54,90,17)	0.90

[a] The following parameters for Cr^{3+} were used: $^1/_3$ Tr $\tilde{g}_2 = 1.98$, $D_2 \approx 0.0$ cm^{-1}, $E_2 \approx 0$. [b] The parameters δ_{Fe} and ΔE_Q for Fe^{2+} are the same as those given in Table 2. [c] The orbital reduction factor (k) and the spin−orbit constant (λ) are used to calculate the anisotropy of $\tilde{g}_1$.[26] [d] Euler angles that rotate the principal axes of $\tilde{D}_1$, $\tilde{g}_1$, and $\tilde{a}_1$ into those of $\tilde{P}_1$. [e] Taken from Chaudhuri *et al.*[2]

spectrum. The success of the simulations confirms the antiferromagnetic spin coupling of Fe^{2+} with Cr^{3+} in **A**. Since the spin degeneracy of the $\mathbf{S}^{eff} = {}^1/_2$ doublet is lifted by the Zeeman interaction ($\beta \mathbf{S}^{eff} \cdot \tilde{g}^{eff} \cdot \mathbf{H}$), Mössbauer spectra are sensitive to the values of $\tilde{g}^{eff}$ for high external fields (e.g., 4.4 T) but are relatively insensitive to small variations of $\tilde{g}^{eff}$ for weak external fields. For our simulations of 2.2 and 4.4 T spectra we used $^1/_3$ Tr $\tilde{g}^{eff} \approx 2.00$, compatible with the EPR data.

We can rationalize the magnitude of $^1/_3$ Tr $\tilde{g}^{eff}$ by relating it to the values of $\tilde{g}_1$ and $\tilde{g}_2$ in the intrinsic representation. Due to spin−orbit coupling we expect the intrinsic tensor $\tilde{g}_1$ for Fe^{2+} to have an average value greater than the spin only value.[26,31] In fact, we found that the simulations are compatible with $^1/_3$ Tr $\tilde{g}_1 \approx 2.07$ (Table 3). For Cr^{3+}, the octahedral component of the crystal field splits the 7-fold orbital degeneracy of its ^{4}F ground state into a lower singlet and two higher triplets. Within the limits of crystal field theory, the electronic density of the orbital singlet has cubic symmetry even in the presence of a tetragonal distortion and the ZFS is small[32] (e.g., $|D_2| \lesssim 1$ cm^{-1} for a variety of Cr^{3+} complexes[25]). The intrinsic tensor $\tilde{g}_2$ is expected to be nearly isotropic (i.e., a scalar),[32] with calculated and experimental values for many Cr^{3+} complexes on the order of $1.96 \lesssim g_2 \leq 1.98$.[25,32−34] Therefore, the first-order relation (eq 8) yields $^1/_3$ Tr $\tilde{g}^{eff} \approx 2.16$ ($^1/_3$ Tr $\tilde{g}_1 \approx 2.07$ and $^1/_3$ Tr $\tilde{g}_2 \approx 1.98$), which is larger than the value inferred from EPR. This can be understood since expression 8 does not take into account the effects of the ZFS on the eigenstates of H_{ex}. The appreciable ZFS from Fe^{2+} perturbs the weak exchange interaction and mixes its ground state with higher spin manifolds, giving rise to low $\tilde{g}^{eff}$ values.[21,26,35] For example, EPR $\tilde{g}^{eff}$ tensors with components lower than the spin-only value are characteristic of the spin ground states of some mixed-valence diiron−oxo proteins,[8,9] such as reduced uteroferrin[31,36] and semimethemerythrin.[37]

Mössbauer spectra are very sensitive to the signs and magnitudes of the magnetic hyperfine tensors. We found that $\tilde{A}_1^{eff}$ is very anisotropic, and simulations of variable applied field spectra confirm its negative sign. This in turn indicates that the internal field, with sign equal to that of the Fermi contact contribution, opposes the external field. From eq 9 we obtained with $^1/_3$ Tr $\tilde{A}_1^{eff}/g_n\beta_n \approx -16.3$ T (Table 2) an estimate of the magnitude of the intrinsic ferrous tensor, $^1/_3$ Tr $\tilde{a}_1/g_n\beta_n \approx -8.2$ T. This value is of the same sign but much smaller than the Fermi contact term for free ions, which is expected to be on the order of −22 T.[38]

Intrinsic Representation. The simulations obtained in the intrinsic representation of eq 2 (not shown) were of equivalent quality as those presented in Figures 2a,b. For the intermediate coupling regime of **A**, to obtain accurate values for the intrinsic parameters, it was necessary to calculate Mössbauer spectra in the intrinsic representation by diagonalization of the $(2S_1 = 5) \times (2S_2 = 4)$ matrix of eq 2. The results are presented in Table 3. Due to the appreciable strength of the ferrous ZFS, the Mössbauer simulations were sensitive to D_1 and E_1. We found that $|J/D_1| \approx 5.3$. In the search for the parameters presented in Table 3, we constrained the value of J to be 21 cm^{-1} as previously estimated from magnetic susceptibility.[2]

As indicated in Table 3, diagonalization of eq 2 also allowed us to determine the intrinsic hyperfine tensor. Here, by including the admixture of spin states due to the ZFS, we found $\tilde{a}_1/g_n\beta_n = -(10.2,3.5,15.6)$ T, $^1/_3$ Tr $\tilde{a}_1/g_n\beta_n \approx -9.8$ T, about 20% larger than the value estimated from eq 9. The ferrous hyperfine tensor is composed of three main components: the dominant isotropic Fermi contact, the anisotropic orbital term, and the anisotropic dipolar term[21,32]

$$a_{ii} = P[-\kappa + (g_{ii} - 2) + {}^1/_{14}\langle L_{ii}^2 - 2\rangle] \qquad (19)$$

where the Fermi contact $-P\kappa$ is negative and determines the sign of the hyperfine tensor. The low value for $^1/_3$ Tr $\tilde{a}_1$ found here indicates that a large orbital component $P(g_{ii} - 2)$ opposes the Fermi contact term (since $^1/_3$ Tr $\tilde{g}_1 > 2$) and reduces the trace of $\tilde{a}_1$. The dipolar term $P/14\langle L_{ii}^2 - 2\rangle$ is evaluated for the ferrous ground state ψ_1 and, being traceless, does not affect the magnitude of $^1/_3$ Tr $\tilde{a}_1$. By using the parameters expected for Fe^{2+} ($P \approx 56$ T,[21] $\kappa = 0.35$,[39] and $^1/_3$ Tr $\tilde{g}_1 \approx 2.07$ (Table 3)), we found from eq 19 $^1/_3$ Tr $a_1 \approx -15.7$ T, which is larger than the empirical value. This suggests that the Fermi contact term for **A** is lower than expected for ferrous ions in ionic environments and that, due to covalency, the values for P and κ used here do not allow an accurate calculation.

It is of interest to see how the components of the hyperfine tensor in effective and intrinsic representations relate to each other. From Tables 2 and 3 we obtained $A_{1x}^{eff}/a_{1x} \approx 1.79$, $A_{1y}^{eff}/a_{1y} \approx 1.60$, and $A_{1z}^{eff}/a_{1z} \approx 1.60$. These ratios differ from those predicted by the strong coupling expression (eq 9), namely, $A_{1i}^{eff}/a_{1i} = 2$. The rotations that determine the relative orientation of the EFG tensor with respect to the hyperfine interaction found in the intrinsic representation (Table 3) were consistent with (i.e., similar to) those found in the effective formalism (Table 2).

Complex B: $Fe^{3+}-\mu O-Cr^{3+}$. In zero field at 4.2 K, the iron site of complex **B** displayed a doublet (Figure 3) with parameters $\delta_{Fe} = 0.52$ mm/s and $\Delta E_Q = -2.00$ mm/s. Although the measured isomer shift is characteristic of the high-spin ferric state,[27−29] the quadrupole splitting is unusually large as found in other Fe^{3+} sites of spin-coupled diiron−oxo proteins.[9] For instance, high-spin ferric sites of reduced uteroferrin, ribonucleotide reductase, and diferric forms of hemerythrin display values for $|\Delta E_Q| \approx 1.93$ mm/s,[21,26,40] ≈ 2.45 mm/s,[41,42] and ≈ 1.95

(31) Day, E. P.; David, S.; Peterson, J.; Dunham, W.; Bonvoisin, J.; Sands, R.; Que, L., Jr. *J. Biol. Chem.* **1988**, *263*, 15561.
(32) Abragam, A.; Price, M. H. L. *Proc. R. Soc.* **1951**, *A205*, 135.
(33) Wertz, J. E.; Bolton, J. R. *Electron Spin Resonance*; Chapmam and Hall: New York, 1986.
(34) Fiorani, D.; Viticoli, S. *Solid State Commun.* **1979**, *30*, 889.
(35) Sage, J. T.; Debrunner, P. G. *Hyperfine Interact.* **1986**, *29*, 1399.
(36) Antanaitis, B. C.; Aisen, P.; Lilienthal, H. R.; Roberts, R. M.; Bazer, F. W. *J. Biol. Chem.* **1980**, *255*, 11204.
(37) Muhoberac, B. B.; Wharton, D. C.; Jensen, L. H.; Harrington, P.; Wilkins, R. G. *Biochim. Biophys. Acta* **1980**, *626*, 337.
(38) Watson, R. E.; Freeman, A. J. *Phys. Rev.* **1961**, *123*, 2027.
(39) Lang, G.; Marshall, W. *Proc. Phys. Soc.* **1966**, *87*, 3.
(40) Rodriguez, J. H.; Ok, H.; Hinrichs, B. E.; Xia, Y. M.; Debrunner, P. G. *Bull. Am. Phys. Soc.* **1993**, *38*(1), 119.
(41) Atkin, C. L.; Thelander, L.; Reichard, P.; Lang, G. *J. Biol. Chem.* **1973**, *248*, 7464.

mm/s,[43,44] respectively, at 4.2 K. We consider that the large ΔE_Q for ferric sites in **A** and diiron−oxo proteins arises from a complex admixture of the following sources. First, it arises from aspherical distributions of charge of the ligand sphere which produce an electric field gradient at the iron site. In particular, the oxo bridge, which is separated from Fe^{3+} by 1.79 Å, introduces some electric field gradient. Second, due to the short bond distances between bridging ligands and metal ions, covalency modifies the valence electron configuration of Fe^{3+}. As indicated in section II, an anisotropic electron population of the valence molecular orbitals centered around the iron produces an electric field gradient which can enhance the quadrupole splitting.

There is no magnetic hyperfine splitting in zero field at 4.2 K as expected for the integer spin ground state $S^{\text{eff}} = 1$. The presence of an external field gives rise to magnetic structure as can be seen in Figures 3 and 4. Spectra recorded in fields of 0.22 to ≈4.7 T at 4.2 K were fitted assuming slow spin relaxation. The relatively broad outer features of the 0.96 and 1.9 T spectra (Figure 4) contrast with the sharper features of the simulations indicating that slow relaxation has not been completely achieved. In a 4.7 T field, data and simulations match very closely, thus indicating slow relaxation.

As mentioned earlier, the solution samples of **A** contained 22% of a ferric complex with Mössbauer parameters similar to those of **B**. This admixture permitted us to see the different effects of increasing temperature on the relaxation rates for high-spin Fe^{2+} and Fe^{3+}. In a 4.7 T field, as we raised the temperature from 4.2 K to approximately 15 K, Fe^{2+} relaxed faster than Fe^{3+}. Qualitatively, at 15 K Fe^{2+} displayed an intermediate to fast relaxation rate whereas Fe^{3+} displayed a slow to intermediate relaxation rate. This difference in behavior can be understood since the orbital singlet high-spin ferric ion lacks orbital angular momentum and therefore couples only weakly to the thermal lattice vibrations. Fe^{3+} can therefore remain in slow relaxation up to relatively high temperatures.

A $S^{\text{eff}} = 1$ Hamiltonian permitted characterization of the spectra, thus confirming antiferromagnetic coupling of Fe^{3+} with Cr^{3+}. From eq 5 it follows that the triplet ground state is well separated from the next higher multiplet, a spin quintet, by[3] $2J \approx 550\ \text{cm}^{-1}$. Since the metal ions are strongly coupled, we expect expressions 10 and 11 to apply. It was possible to fit the experimental data with a nearly isotropic tensor $\tilde{g}^{\text{eff}} = (1.99, 2.02, 2.02)$, $^1/_3\ \text{Tr}\ \tilde{g}^{\text{eff}} = 2.01$, that approximately results from expression 10 if $^1/_3\ \text{Tr}\ \tilde{g}_1 \approx 2$ and $^1/_3\ \text{Tr}\ \tilde{g}_2 \approx 1.98$.[25,32−34]

Fe^{3+} has a half-filled d shell, which leads to an orbital singlet ground state and hence to an isotropic intrinsic hyperfine tensor $\tilde{a}_1$. We found that the corresponding effective tensor is also nearly isotropic, $\tilde{A}_1^{\text{eff}}/g_n\beta_n = -(33.8, 30.9, 35.8)$ T. Isotropy indicates that the perturbation of the ZFS to the states of H_{ex} ($J \approx 275\ \text{cm}^{-1}$) is very small since $|J/D_{1,2}| \gg 1$. From the average of $\tilde{A}_1^{\text{eff}}/g_n\beta_n$ we calculated from eq 11 the trace of the intrinsic hyperfine tensor $^1/_3\ \text{Tr}\ \tilde{a}_1/g_n\beta_n \approx -19$ T. This estimate is smaller in magnitude than the Fermi contact values of approximately −20 to −22 T expected for many Fe^{3+} compounds.[45] Since the calculated intrinsic trace was lower than expected, we searched in the parameter space of Hamiltonian 6 with the constraint that $\tilde{A}_1^{\text{eff}}/g_n\beta_n = -(36.8, 36.8, 36.8)$ T, which is calculated from eq 11 for an intrinsic tensor with components of ≈−21 T, as found in many ferric compounds. We found that such a constraint did not permit a successful simulation of the spectra and it was necessary to allow $\tilde{A}_1^{\text{eff}}$ to vary in an optimization procedure and eventually acquire the values presented in Table 2.

The relatively low value of the trace of $\tilde{a}_1$ implies a reduced net s-electron spin density at the nucleus with respect to that of other Fe^{3+} ions with larger Fermi contact fields. We have previously reported an intrinsic $\tilde{a}_1$ tensor with a low component ($a_{1z} \approx -17.8$ T) for the ferric site of the diiron−oxo center of reduced uteroferrin.[21,40] This suggests that there is a tendency for ferric ions in diiron−oxo centers to display somewhat lower hyperfine splittings than those of monomeric ions.

For a free Fe^{3+} ion, Freeman and Watson[38,46] find a theoretical Fermi contact hyperfine field $\mathbf{H}^{\text{c}} = -63.0$ T corresponding to $a_1^{\text{c}}/g_n\beta_n \approx -25$ T. We can interpret this value with the expression

$$a_1^{\text{c}} = \sum_n (a_\uparrow^{\text{c}} - a_\downarrow^{\text{c}})_{\text{ns}} \tag{20}$$

where $(a_\uparrow^{\text{c}} - a_\downarrow^{\text{c}})_{\text{ns}}$ are proportional to the net s spin densities at the nucleus resulting from the 1s, 2s, and 3s shells. The arrows ↑ and ↓ refer to electrons with spin parallel and antiparallel to the 3d shell spin, respectively. For a free ion, the contribution from the 4s shell is nominally zero. In expression 20, the net contributions from 1s and 2s are negative whereas that from 3s is positive.[38,46] For Fe^{3+} ions in a complex, the value of $|a_1^{\text{c}}|$ decreases with respect to the free ion value. In general, data for the isoelectronic ions Mn^{2+} [47] and Fe^{3+} [48] reveal that with increasing covalency the value of $|a_1^{\text{c}}|$ decreases. This fact is consistent with a finite covalent spin density at the 4s shell which produces a positive contact hyperfine field[38,46] and opposes the dominant negative contributions from 1s and 2s. We can conclude that the short $Fe^{3+}-O^{2-}$ bond length (1.792 Å) allows noticeable covalent occupation of the 4s shell in complex **B**. The overlap of O^{2-} 2p orbitals with filled 2s and 3s shells gives rise to unpairing of s electrons at the Fe^{3+} nucleus. This latter effect is greater for the 3s than for the 2s shell.[49] Since $(a_\uparrow^{\text{c}} - a_\downarrow^{\text{c}})_{3s}$ is positive, we also expect a decrease in the magnitude of a_1^{c} due to this overlap effect.

Some covalent 3d bonding also occurs due to 2p → 3d transfer which increases the 3d charge and introduces some EFG. This effect explains, at least in part, the large quadrupole splitting observed. The covalent occupation of d orbitals can introduce some minor orbital and traceless dipolar contributions to the hyperfine tensor which can also reduce its trace and introduce some anisotropy. These latter effects are consistent with the small anisotropy observed for $\tilde{A}_1^{\text{eff}}$. The importance of 4s and 3d covalent bonding has been pointed out previously[46,50] for the case of Fe^{3+} salts.[49,51]

Figures 3 and 4 show that the magnetic splitting increases for larger applied fields in contrast to what is normally observed for monomeric Fe^{3+} with a negative internal field that opposes the external field. This behavior is related to the integer spin $S^{\text{eff}} = 1$ of the complex. The zero field eigenstates of integer

(42) Lynch, J. B.; Juarez-Garcia, C.; Münck, E.; Que, L., Jr. *J. Biol. Chem.* **1989**, *264*, 8091.
(43) Okamura, M. Y.; Klotz, I. M.; Johnson, C. E.; Winter, M.; Williams, R. J. P. *Biochemistry* **1969**, *8*, 1951.
(44) Garbett, K.; Johnson, C. E.; Klotz, I. M.; Okamura, M. Y.; Williams, R. J. P. *Arch. Biochem. Biophys.* **1971**, *142*, 574.
(45) Srivastava, J.; Bhargara, S.; Iyengar, P.; Thosar, B. In *Advances in Mössbauer Spectroscopy*; Thosar, B., Iyengar, P., Eds.; Elsevier: New York, 1983.
(46) Freeman, A. J.; Watson, R. E. In *Magnetism*; Rado, G. T., Suhl, H., Eds.; Academic Press: New York, 1965; Vol. IIA, Chapter 4, pp 167−305.
(47) Matumura, O. *J. Phys. Soc. Jpn.* **1959**, *14*, 108.
(48) Henning, J. *Phys. Lett.* **1967**, *24A*, 40.
(49) Šimáneck, E.; Šroubek, Z. In *Electron Paramagnetic Resonance*; Geschwind, S., Ed.; Plenum Press: New York, 1972.
(50) Sawatsky, G. A.; Woude, F. V. D. *J. Phys. Colloq.* **1974**, *35*, C6−47.
(51) Šimáneck, E.; Šroubek, Z. *Phys. Rev.* **1967**, *163*, 275.

spin systems yield vanishing spin expectation values, and it is the Zeeman mixing of states that produces finite spin expectation values. As the external field mixes the states and induces spin polarization, the internal field increases in magnitude since it is directly proportional to $\langle S^{\text{eff}} \rangle$ through the relation

$$\mathbf{H}_{\text{int}} = -\langle \mathbf{S}^{\text{eff}} \rangle \cdot \frac{\tilde{A}^{\text{eff}}}{g_n \beta_n} \tag{21}$$

The net field at the iron nucleus is the vector sum of internal and external fields. For Fe^{3+} the Fermi contact field, which is negative and isotropic, is to first order the only source of internal field. We found that, within the range of external fields used in our study, the spin expectation values $\langle S_x \rangle$, $\langle S_y \rangle$, and $\langle S_z \rangle$ do not saturate. We calculated expectation values for the components of the effective spin along its three principal axes by diagonalizing the electronic part of eq 6. Due to the large rhombic contribution from the ZFS, the $\langle S_y \rangle$ component approaches fastest the saturation value of $S^{\text{eff}} = -1$ with increasing external field. Here, the net field increases with external field since an increment of positive external field is smaller than the corresponding negative increment of internal field due to spin polarization.

Effect of Main Bridging Ligands on Spin Coupling. The complexes **A** ($Fe^{2+}-OH-Cr^{3+}$) and **B** ($Fe^{3+}-O-Cr^{3+}$) differ in their main bridging ligands and the oxidation state of the iron ions. At the same time, the exchange constant is about an order of magnitude lower for **A** than for **B**. We now briefly discuss the origin of the difference in the strength of spin coupling and its correlation with the type of bridging ligand or iron oxidation state.

The greater ability of oxide to form covalent bonds than hydroxide reflects in their respective Fe−O bond lengths and strength of spin coupling between the metal ions. For **A**, the $Fe^{2+}-OH^-$ bond length is 2.037 Å and $J \approx 21$ cm^{-1}. In contrast, **B** has an $Fe^{3+}-O^{2-}$ bond length of 1.792 Å and $J \approx 275$ cm^{-1}. The Fe−Cr complexes studied here show the tendency for oxide to form dinuclear centers with shorter bonding lengths and larger coupling strengths than hydroxide. This correlation between bridging ligand, bond length, and spin coupling strength has been observed in several model compounds. For example, protonating the μ-oxo bridge in differic models for met-hemerythrin,[3,52] without reducing the iron, decreases by nearly an order of magnitude their coupling constant and increases their Fe−O bond lengths. In these complexes the large difference in coupling strength between μ-oxo and μ-hydroxo bridged diiron centers is related to the type of bridging ligand and not to the iron oxidation state, which remains unchanged.

The similar dependence of the coupling strength on the type of bridging ligand observed for some homobinuclear ($Fe^{3+}-Fe^{3+}$)[3,52] and for the heterobinuclear ($Fe^{3+}-Cr^{3+}$, $Fe^{2+}-Cr^{3+}$) complexes studied here suggests that, for coupled iron and chromium, the magnitude of J depends mostly on the nature of the bridging ligands (i.e., oxide or hydroxide) and not as much on the oxidation state of the iron ions. The previous observation can be rationalized since the magnitude of J strongly depends on the metal−metal distances,[53,54] which are related to the type of bridging ligand, and to the main antiferromagnetic exchange pathways involved.[55] Hotzelmann *et al.*[3] have identified three main antiferromagnetic pathways for their μ-oxo bridged $Fe^{3+}-Fe^{3+}$ complex, and two main pathways for the μ-oxo bridged $Fe^{3+}-Cr^{3+}$ complex (**B**) studied here. In particular, the strong antiferromagnetism of **B** is ascribed[3] to contributions corresponding to the Fe^{3+}:$d_{z^2} \leftrightarrow d_{xz}$:$Cr^{3+}$ and Fe^{3+}:$d_{yz} \leftrightarrow d_{yz}$:$Cr^{3+}$ pathways, which are also main contributors in the diferric complex. The magnetic character of neither of these pathways is significantly affected by reducing the iron to the ferrous state since the extra electron of Fe^{2+} is paired, giving rise to a nonmagnetic ground state $d^{\uparrow\downarrow}_{x^2-y^2}$ orbital (with respect to an orthorhombic coordinate system)[3] which is not significantly involved in antiferromagnetic coupling. Therefore, a change in oxidation state from Fe^{3+} to Fe^{2+} should not drastically alter the magnitude of J as long as the main bridging ligand and exchange pathways remain the same.

The trends stated above are relevant when one is trying to elucidate the type of bridging ligand present in diiron−oxo proteins with unknown crystallographic structure. For example, reduced uteroferrin, a purple acid phosphatase from pig allantoic fluid, is a protein with a mixed-valence $Fe^{3+}-Fe^{2+}$ center, unknown crystallographic structure, and a coupling constant on the order of $J \approx 35$ cm^{-1}.[21] The magnitude of J is a strong indicator of a bridging hydroxide in reduced uteroferrin. Furthermore, in some cases, the presence of the hydrogen in the bridging OH^- cannot be unambiguously determined from crystallography. Sträter *et al.*[56] have crystallographically characterized the iron−zinc center of kidney bean purple acid phosphatase (KBPAP) at a resolution of 2.9 Å. At this resolution, the electron density map reveals no unambiguous indication of H_2O, OH^-, or O^{2-} ligands coordinated to the metal sites. The Fe−O and Zn−O distances in KBPAP are 1.9 and 2.1 Å, respectively.[56] On the basis of the geometry of the coordination sphere around the metal ions these authors have proposed the presence of a μOH^- bridge for KBPAP, consistent with the trends stated here based on the bond lengths.

VI. Conclusion

We briefly summarize some of our findings and conclusions.

(i) Effective $S^{\text{eff}} = {}^1/_2$ and $S^{\text{eff}} = 1$ Hamiltonians successfully reproduce 4.2 K spectra from complexes **A** and **B**, respectively.

(ii) The spin coupling is weak for complexes **A**; however, this does not affect significantly the validity of the $S^{\text{eff}} = {}^1/_2$ Hamiltonian for $T \lesssim 7$ K. The use of the $S^{\text{eff}} = {}^1/_2$ representation is valid at low temperatures since only the ground doublet is significantly populated for $Fe^{2+}-OH-Cr^{3+}$.

(iii) In order to determine intrinsic parameters for the Fe^{2+} site of **A**, it was necessary to account for the mixing of states corresponding to higher spin manifolds (e.g., $S = {}^3/_2$) with the Kramers doublet ground state. Such an admixture results mostly from the perturbation of the Fe^{2+} ZFS on the exchange interaction since $|J/D_1| \approx 5.3$ and $|J/D_2| \gg 1$. The ZFS parameters for Fe^{2+} are positive, indicating that the singlet substate of the $S_1 = 2$ manifold is the ground state.

(iv) The magnitude of the trace of $\tilde{a}_1$ for the Fe^{3+} site of complex **B** is smaller than expected for many ferric complexes. This indicates that the 4s shell has a net spin density which results in a positive contribution to the isotropic Fermi contact field. The small anisotropy of $\tilde{A}_1^{\text{eff}}$ for **B** suggests that minor orbital and dipolar components contribute to the ferric tensor $\tilde{a}_1$.

(v) The Fe^{3+} site of complex **B** has a quadrupole splitting $\Delta E_Q = -2.00$ mm/s at 4.2 K, which is unusually large for a high-spin ferric ion. Similarly large quadrupole splittings have

(52) Armstrong, W. H.; Lippard, S. J. *J. Am. Chem. Soc.* **1984**, *106*, 4632.
(53) Scaringe, R. P.; Hodgson, D. J.; Hatfield, W. E. *Transition Met. Chem.* **1981**, *6*, 340.
(54) Gorun, S. M.; Lippard, S. J. *Inorg. Chem.* **1991**, *30*, 1625.
(55) Ginsberg, A. P. *Inorg. Chim. Acta, Rev.* **1971**, *5*, 45.
(56) Sträter, N.; Klabunde, T.; Tucker, P.; Witzel, H.; Krebs, B. *Science* **1995**, *268*, 1489.

been measured for ferric sites in a number of diiron−oxo proteins such as ribonucleotide reductase,[41,42] uteroferrin,[21,26,40] and diferric forms of hemerythrin,[43,44] all of which have μ-oxo or μ-hydroxo bridged antiferromagnetically coupled iron centers. The large ΔE_Q is related to the combined effects of anisotropic covalency and the aspherical charge from the ligand sphere.

(vi) In complexes **A** and **B**, at 4.2 K the iron sites reach the limit of slow relaxation only when relatively high magnetic fields are applied. In contrast, for several $Fe^{3+}-Fe^{2+}$ centers (e.g., reduced uteroferrin[26]), slow relaxation is achieved for low field intensities (e.g., 0.032 T). This fact indicates that $Fe^{2+}-Cr^{3+}$ and $Fe^{3+}-Cr^{3+}$ pairs tend to exhibit faster relaxation than diiron pairs.

Acknowledgment. This work was supported in part by NIH Grant GM 16406. The award of an IAEA fellowship to J.H.R. is acknowledged.

JA952513P